Chemical Engineering Science 260 (2022) 117927

Contents lists available at ScienceDirect

Chemical Engineering Science

journal homepage: www.elsevier.com/locate/ces

Experimental study on the effects of particle characteristics and pressurization methods on powder compression

Shicheng Wang, Xiaolei Guo *, Haifeng Lu, Haifeng Liu *

National Energy Research Center of Coal Gasification Technology, Shanghai Engineering Research Center of Coal Gasification, East China University of Science and Technology, P. O. Box 272, Shanghai 200237, PR China

HIGHLIGHTS

- The difference in compressibility caused by particle characteristics and pressurization methods were analyzed.
- The relationship between normal stress and gas pressurization rate was proposed.
- The mechanism of different pressurization methods was discussed.

ARTICLE INFO

Article history:
Received 5 April 2022
Received in revised form 14 July 2022
Accepted 17 July 2022
Available online 21 July 2022

Keywords:
Gas pressurization
Powder compression
Particle characteristics

ABSTRACT

Both the particle characteristics and the pressurization methods have an important influence on powder compression behavior. Compression of powder with different average particle sizes, sphericity and adhesion were experimentally investigated by the FT4 rheometer and the pressurized visualization tank. The difference in compressibility caused by particle characteristics and pressurization methods were analyzed. The results show that the smaller the average particle size, the higher the sphericity and the greater the adhesion, the greater the compressibility of the powder. In the experimental range, the effect of gas pressurization is less than mechanical pressurization on powder compression. The relationship between normal stress and gas pressurization rate was proposed and the mechanism of different pressurization methods was also discussed with compression position and mode.

1. Introduction

Powder compression has a wide range of industrial applications, including gas pressurization in silos (Lu, H. et al., 2012), pharmaceutical powder compression (Kaerger et al., 2004), ceramic processing (Saha et al., 2012), metallurgical engineering (Bombac et al., 2020), etc. Powder compaction and densification refer to the process in which the bulk density of a powder under natural packing conditions increases and achieves a high degree of densification under the transient action of external forces (Richard et al., 2005). During this process, the mesh structure of the particles supports the applied load. For irregular packing, the contact forces between the particles change. The particles rearrange themselves under these forces and increase their density by sliding into the voids with each other (Kuhn et al., 1991).

The macroscopic properties of powder compression are the joint result of microscopic interactions between particles. Particle properties include particle size, particle size distribution, particle shape, angle, hardness and surface roughness (Sukumaran and Ashmawy, 2003).

Samimi et al found through experiments and simulations that the Heckle and Kwakita parameters decreased with increasing particle size, which indicated that larger particles were easier to compact (Samimi et al., 2005). Powders with a wider particle size distribution have greater void fraction and more relative density variation during compression. They are easier to compress because finer particles can fill the gaps between larger particles (Adolfsson et al., 1997; Koynov et al., 2013; Shen et al., 2022).

The description of particle shape includes sphericity, convexity and aspect ratio. Particle shape has a significant effect on strength, with higher sphericity resulting in higher average strength (Zhu and Zhao, 2021). Compared with spherical particles, tetrahedral particles were less compressible due to enhanced shear resistance to interparticle contact, reduced particle rearrangement in the early stages of overall compression, and enhanced resistance to overall deformation in the later stages (He and Guo, 2018). Abdullah and Geldart proved that the more spherical shaped FCC

* Corresponding authors.
E-mail addresses: gxl@ecust.edu.cn (X. Guo), hfliu@ecust.edu.cn (H. Liu).

https://doi.org/10.1016/j.ces.2022.117927
0009-2509/

mixtures had a greater packing state than the more angular shaped FRF mixtures (Abdullah and Geldart, 1999). The greater the non-convexity of the particles, the more contact between the particles, resulting in higher compressive strength particle interlocking (He et al., 2019).

In the microscale, the compressibility of the powder was influenced by the adhesion and friction forces between the particles (Stasiak et al., 2010). Abdullah and Geldart showed that free-flowing powders had a low tendency to consolidate (Abdullah and Geldart, 1999). Tomas proposed ultra-fine cohesive powders were characterized by low flowability and high compressibility (Tomas, 2007).

Mechanical pressurization is the most common way of powder compression, where compressibility is tested by applying mechanical thrust to the powder. The main tests of powder compressibility were the uniaxial compression experiment (Stasiak et al., 2010), solidification meter experiment (Yigit, 2018) and compression test unit in FT4 powder rheometer (Zeng and Wang, 2019), etc. These tests provide an important reference for the compressive properties of powders under mechanical stress. Gas can also have a compressive effect on the powder. In the high-pressure hopper discharging unit for pulverized coal, the compaction of pulverized coal is difficult to discharge due to the increase in hopper pressure (Lu, H. et al., 2012). Jenike proposed that the gas pressure gradient in the process of gas pressurization in the hopper increased the degree of consolidation of the powder bed, increasing the packing density (Jenike, 1983).

In this paper, we experimentally compare the variation of different particle sizes, sphericity and adhesion in the compression process to reveal the effect of particle characteristics on the compression behavior of powders. In order to understand the compression ability of mechanical and gas pressurization on the powder, we compared compression results to provide a further understanding of the compression caused by gas pressurization.

2. Experimental setup

2.1. Materials

In this study, two typical powders (Alumina, Glass beads) were used in the experiments where A, B, C, D are alumina, E is glass beads. The physical properties of experimental materials are shown in Table 1. Sauter mean diameters (d_p) were measured by the particle size analyzer (Malvern Mastersizer 2000MU). Particle density (ρ_p) was measured by the true density analyzer (Quantachrome 1200e). Bulk density (ρ_b) and Tap density (ρ_t) were measured by the PT-X (Hosokawa Micron Corporation). The values of the *HR* (Hausner Ratio) and the compressibility (C) of different samples were obtained by calculation ($HR = \frac{\rho_t}{\rho_b} = \frac{1}{1-C}$), and the conclusion showed that A > B≈C > E > D. Fig. 1 reports that the particle size distribution of the experimental samples is relatively concentrated and its effect can be ignored.

The particle morphology of the experimental material was analyzed by using Camsizer XT and the relevant parameters were shown in Table 2. Sphericity is defined as the ratio of the surface area of a sphere having the same volume as the particle to the surface area of the particle. The samples A, B, D and E are spherical and C is non-spherical. To further confirm and analyze the particle morphology of the experimental material, we used SEM (SU1510, HITACHI) to obtain the microscopic morphological features as shown in Fig. 2. It can be clearly observed that C is irregularly blocky and the rest of the material is spherical.

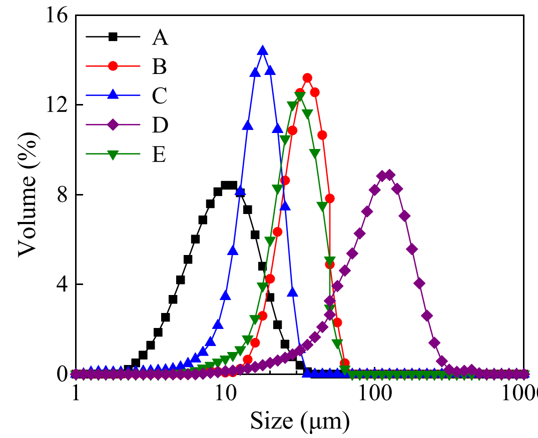

Fig. 1. Particle size distribution.

Table 2
Particle morphology parameters.

Material	Mean Sphericity	Aspect ratio	Convexity
A	0.955	0.930	0.998
B	0.956	0.931	0.994
C	0.874	0.719	0.989
D	0.931	0.944	0.996
E	0.969	0.954	0.996

2.2. Apparatus and methods

2.2.1. Mechanical pressurization test

Powder mechanical pressurization test equipment is given in Fig. 3. To obtain a more quantitative characterization of the powder compression properties, the FT4 powder rheometer (Freeman Technology) was used to conduct the compression test with a mechanical piston. The diameter of the glass tube is 50 mm, whose volume is 220 ml. The normal stress of 0 KPa – 15 KPa is gradually applied to the powder by the piston, each normal stress is applied for a defined time to allow the powder to reach equilibrium. The distance travelled by the piston is measured for each applied normal stress and the compressibility is automatically calculated as a percentage change in volume.

2.2.1.1. Gas pressurization test. The experimental equipment mainly consists of a gas supply system, a gas volume regulation system, a pressurization system and a real-time data collection system, as shown in Fig. 4. The height of the glass tube is 200 mm, diameter

Table 1
Physical properties of experimental samples.

Material	d_p(μm)	ρ_p(kg/m^3)	ρ_b(kg/m^3)	ρ_t(kg/m^3)	*HR*	*C*
A	8.68	3900.0	1547.9	2383.9	1.54	0.35
B	31.75		1933.6	2410.1	1.25	0.20
C	27.43		1521.4	1919.1	1.26	0.21
D	87.85		2220.8	2372.4	1.07	0.07
E	33.14	2491.1	1370	1591.5	1.16	0.14

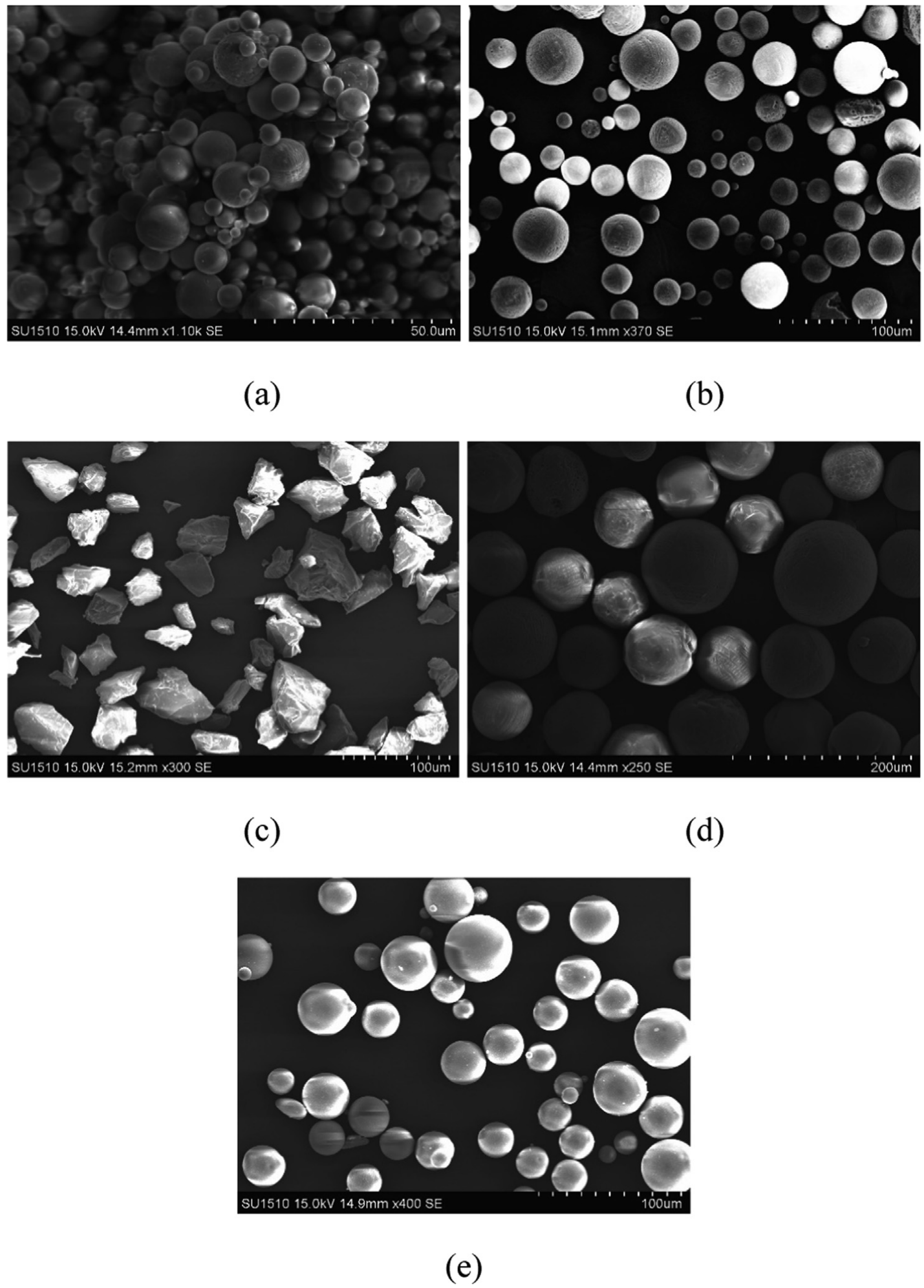

Fig. 2. SEM image of experimental samples: (a) A; (b) B; (c) C; (d) D; (e) E.

is 30 mm. The pressurization rate of the visualization tank can be controlled by a needle valve and the final tank pressure is set at 1 Mpa. The camera can record the variation of the powder bed height in real time. The Adobe Premiere software was used to process the video with a single image resolution of 2592 × 1944 and 5 megapixels. The height variation of the powder bed was calibrated using ImageJ software with an accuracy of 0.01 mm. As a result, both the compressibility percentage and compaction density can be calculated according to the height variation.

In the above two tests, all powders were dried at 105 °C to remove the effect of moisture content. At the same time, the way of filling the powder into the glass tube was kept consistent to reduce the influence of the initial packing state on the experimental results.

3. Results and discussion

3.1. Mechanical pressurization test results

The compressibility percentage under different normal stresses was obtained, as shown in Fig. 5.

Comparison of the spherical alumina A, B and D, we observed that the smaller the average particle size, the greater the compress-

Fig. 3. FT4 mechanical pressurization test unit.

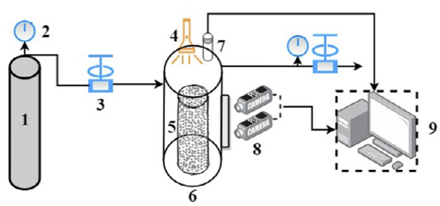

1 - Nitrogen cylinder; 2 - Pressure gauge; 3 - Needle valve;

4 - Lighting fixture; 5 - Glass tube; 6 - Visualization tank; 7 - Pressure sensor;

8 - Cameras; 9 - Computer

Fig. 4. Diagram of the gas pressurization experimental set-up.

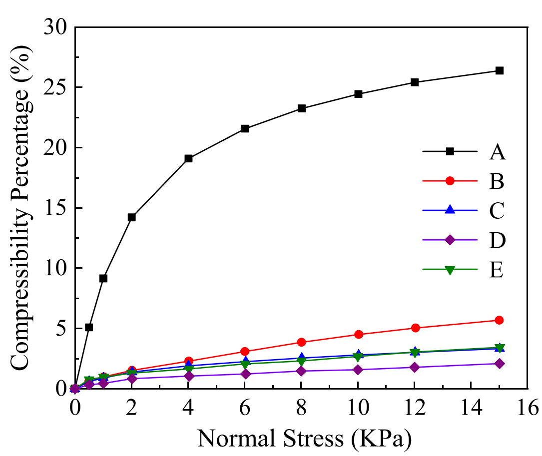

Fig. 5. Mechanical pressurization test.

ibility when the particle shape is the same. Especially for A (d_p = 8.68 μm), the compressibility is much higher than B (d_p = 31.75 μm) and D (d_p = 87.85 μm). At normal stress of 15 KPa, the compressibility of A is 26.4 %, while the compressibility of B and D is 5.68 % and 2.09 %, and A is 5 times that of B and 13 times that of D. Unlike large particles, the compressibility of fine particles (<100 μm) increases with decreasing particle size.

The particle size is closely related to the interparticle forces, which have an important effect on the void fraction of the powder bed. Guerin (Guerin, 2004) believed that the smaller the particles, the greater the friction, adhesion, and even van der Waals forces compared to gravity. Small particles form agglomerates due to interparticle forces, and agglomeration brings the system to a rather random agglomerate shapes with larger pores. The agglomeration tends more effectively to minimize the energy of the system by increasing its density compared to gravity, leading to greater compressibility.

Comparing spherical alumina B (Mean Sphericity = 0.956) with non-spherical alumina C (Mean Sphericity = 0.874), we found that the higher the sphericity, the greater the compressibility when the mean particle size is the same. When the normal stress is 15 KPa, the compressibility of B is 5.68 %, which is 1.7 times that of C.

The relatively low compressibility of irregular particles is consistent with the results of (Zhu and Zhao, 2021). Zou et al found that the particle shape has an important effect on the initial porosity (Zou and Yu, 1996). In general, decreasing sphericity can increase initial porosity. For high sphericity particles, rearrangement can be easily achieved during the compression process. The above results are caused by a combination of several reasons, such as the higher probability of forming bridges by the angular corners of particles (Haughey and Beveridge, 1969), interparticle friction (RAMAKRISHNAN, 1976; Xu et al., 2001) or surface roughness (German, 1989). In addition, the particle shape has an effect on the interparticle void ratio. As the sphericity decreases, the interparticle void size distribution becomes narrower. The local voids decrease, leading to a decrease in compressibility (et al., 1999). Meanwhile, at equal particle size, the spherical shape provides a locally larger radius of curvature at the interparticle contact points, a result that is directly related to larger interparticle forces.

Zhu et al quantitatively characterized the flowability of both powders by shear tests (Zhu et al., 2022; Zhu et al., 2020). According to the Jenike flow function criteria, alumina is a typical cohesive powder, while glass bead is non-cohesive. Contrasting spherical alumina B and glass beads, we found that the compressibility of spherical alumina was greater than glass bead when the average particle size and sphericity were the same, indicating that the compressibility of cohesive powder was greater than non-cohesive powder.

For dry fine particles, the cohesive forces are mainly van der Waals forces. When the van der Waals force exceeds the gravity, the powder shows adhesion (Sharma and Setia, 2019). Before compression, the packing state of glass beads (non-cohesive) is mainly influenced by gravity, and the particles are closely arranged with each other. Due to the influence of cohesive forces, the packing state of alumina is looser than the glass beads and has higher compressibility. After applying the same normal stress, the effects of the interparticle forces that appear through a powder expanded state are disrupted. The normal stress is in the same direction as gravity, which further increases the particle rearrangement. So the two types of powders with the same particle size and sphericity, the cohesive powder has higher compressibility.

Tomas (Tomas, 2004) derived the powder compression equation based on the Kawakita equation (Kawakita and Ludde, 1971) by the relationship between the total pressure and the interparticle forces in the van der Waals equation, as shown in Eq.(1). The equation describes the relationship between the powder compaction density ρ_b and the normal stress σ_z:

$$\frac{\rho_b}{\rho_{b,0}} = \left[\frac{\sigma_z + \sigma_{z,0}}{\sigma_{z,0}}\right]^N \tag{1}$$

where $\rho_{b,0}$ ias the packing density without normal stress and $\sigma_{z,0}$ is the pull-off stress when the unconfined yield strength is zero. The parameter N is a physics-based compressibility index in the range of 0–1. The larger the N, the greater the compressibility.

The corresponding regression curves obtained from Eq. (1) and the experimental results were given in Fig. 6, which can well describe the variation of compaction density ρ_b and the relative compaction density (RCD) (ρ_b-ρ_0)/ρ_0 under different normal stres-

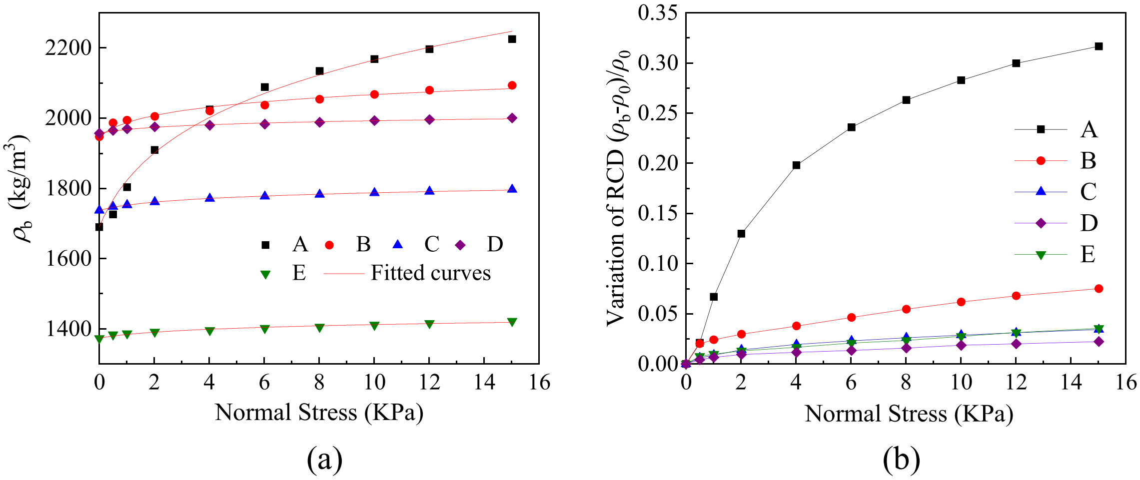

Fig. 6. Variation of compaction density (a) and RCD (b) with normal stress.

ses. The fitting parameters and correlation coefficients were shown in Table 3.

(b).

From the figure, we can observe the initial packing density D > B > C > A > E and variation of RCD A > B > C≈E > D. For all powders, larger particle size, sphericity and adhesion correspond to higher initial packing density. Despite the large variation in the initial packing state, there is little difference in the results of RCD variation during compression.

In order to compare the compressibility of different samples more clearly, the relationship between the compressibility index and compressibility percentage (normal stress is 15 KPa) is given in Fig. 7. The trend of the compressibility index N is consistent with the compressibility percentage. The compressibility of A is much greater than other samples, indicating that particle size is the key to the compressibility of the powder. Compared to particle size, particle shape and adhesion have relatively little effect.

According to Thomas' evaluation of different ranges of compressibility indices (Tomas, 2004), it is found that A belongs to compressible materials (range of N is 0.05–0.1), B, C and E belong to low compressibility materials (range of N is 0.01–0.05), and D belongs to incompressible materials (range of N is 0–0.01), which further verifies the experimental conclusion.

3.2. Gas pressurization test results

With the real-time recording by camera, the height variation of the powder bed during the whole compression process can be observed and the RCD variation with time is calculated, as shown in Fig. 8 (the variation curve of D is removed from the figure because it is difficult to obtain process variation). The powder bed compression process can be divided into a dynamic stage and a final steady-state stage.

At a pressurization rate of 5 KPa/s, the variation RCD of A was 9.56 %, B, C and E were 1.59 %, 0.74 % and 0.62 %, respectively.

Table 3
Fitting parameters and correlation coefficients.

Material	$\rho_{b,0}$/kg·m^{-3}	$\sigma_{z,0}$/Pa	N	R^2
A	1690	860.2	0.098	0.989
B	1947	604.1	0.020	0.968
C	1737	848.7	0.011	0.997
D	1957	839.2	0.007	0.982
E	1374	1149.1	0.012	0.969

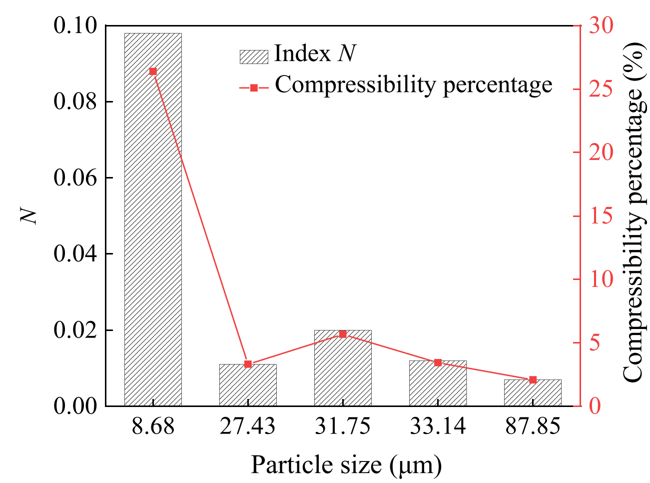

Fig. 7. Compressibility index and percentage (normal stress is 15 KPa) comparison.

The compression process of A ends at 10 s, B, C and D end at about 1 s. The smaller the particle size, the faster the compression rate. Meanwhile, small particles with high RCD take a longer time to reach the steady-state. Increasing the pressurization rate not only increases the variation in the degree of compression among different powders, but also accelerates the time from the dynamic to the steady-state phase of the powder bed.

The compressibility percentage at different pressurization rates is given in Fig. 9. The experimental results show the compressibility A > B > C≈E > D which is consistent with the results of mechanical pressurization. The corresponding regression curves were obtained as shown in Fig. 10, which can well describe the variation of compaction density at different pressurization rates. Compared with mechanical pressurization, the compressibility percentage increases rapidly with increasing pressurization rate and then increases smoothly under gas pressurization. Taking A as an example, the compressibility grows rapidly from 0 KPa/s to 15 KPa/s and slowly from 15 KPa/s to 60 KPa/s.

3.3. Comparison of pressurization methods

Fig. 11 shows the compression results of powders with different particle characteristics under two pressurization methods. When the samples reached the steady-state by the method of mechanical pressurization (normal stress is 15 KPa) and gas pressurization

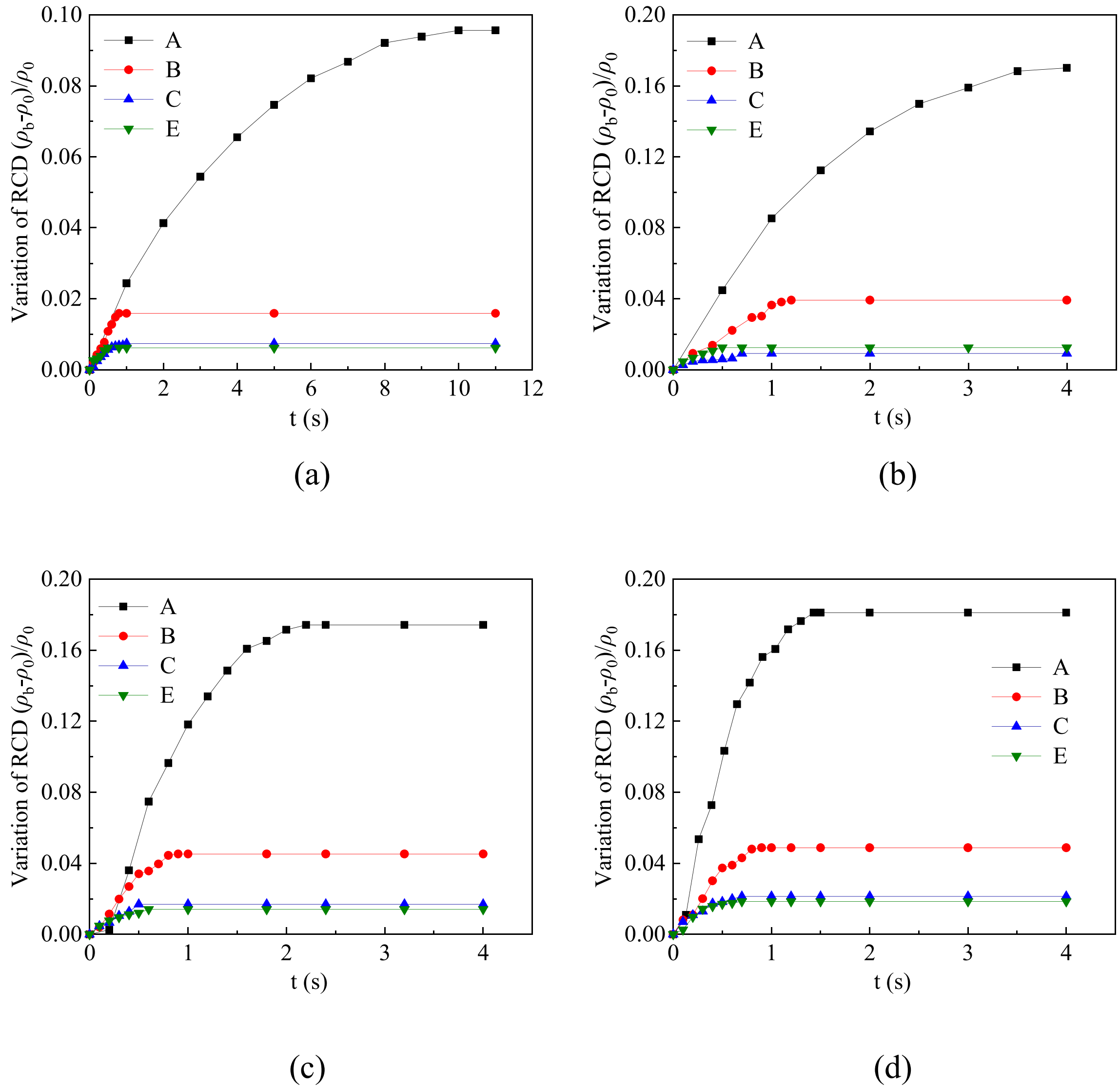

Fig. 8. Variation of RCD $(\rho_b-\rho_0)/\rho_0$ as a function of pressurization time. (a)5 KPa/s; (b)15 KPa/s; (c)40 KPa/s; (d)60 KPa/s.

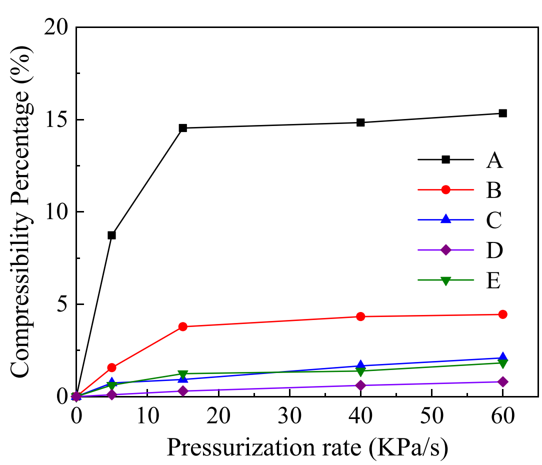

Fig. 9. Gas pressurization test.

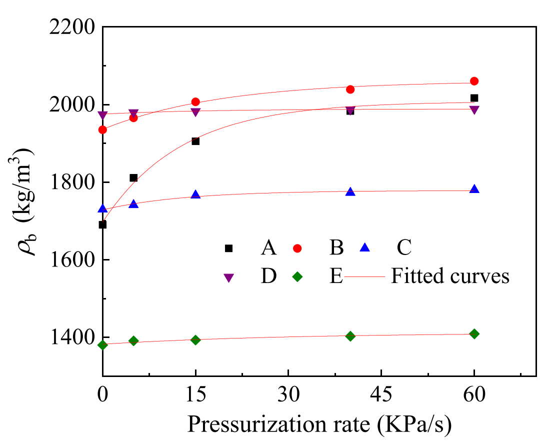

Fig. 10. Variation of compaction density with Pressurization rate.

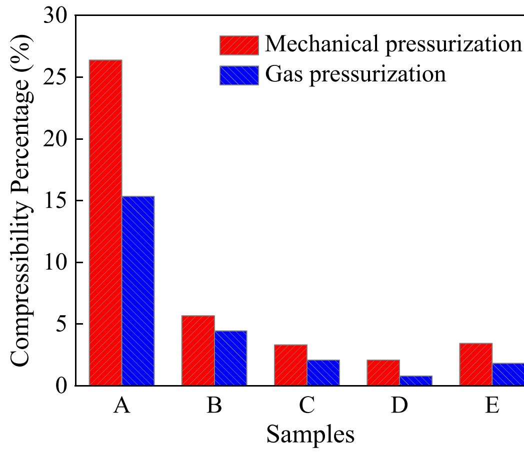

Fig. 11. Mechanical pressurization compared with gas pressurization.

(pressurization rate is 60 KPa/s), respectively, we compared the compressibility percentage.

The difference in small particle size is significant when reaching the steady-state, and the difference in large particle size is little. Because the compressibility of large particles is small, and it is difficult to reflect the compressibility of the two pressurization methods, while small particles can clearly contrast the difference between the pressurization methods. To effectively compare the differences between the two pressurization methods, the equivalent conversion of pressurization rate and normal stress is necessary.

In order to quantify the magnitude of the effect of gas pressurization relative to mechanical pressurization, the relationship curve between the pressurization rate and the normal stress was obtained based on the experimental results in Fig. 5 and Fig. 9 (further calculated to obtain the RCD variation as a way to eliminate the effect of the initial packing density), as shown in Fig. 12.

Since the mechanisms of mechanical pressurization and gas pressurization are different, the normal stresses transformed by the pressurization rate in Fig. 12 are not equal to the actual mechanical pressurization, but " equivalent " stresses. Under the equivalent stress applied by gas, the equivalent effect can be obtained as the normal stress applied by mechanical pressurization. The equivalent stress of the gas is not only related to the pressurization rate, but also influenced by the particle characteristics. The greater the compressibility, the smaller the equivalent stress

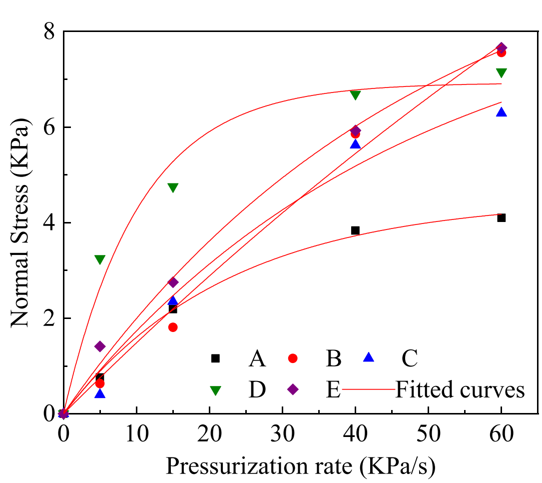

Fig. 12. The relationship between normal stress and pressurization rate.

required. The particle size has a significant effect on the equivalent stress, while the sphericity and the adhesion have almost no effect. The larger the particle size, the greater the equivalent stress corresponding to the same compressibility. Particle characteristics are not the only factors affecting parameters A and B. The bed height or the aspect ratio can also be affecting factors for the different compressibility percentages of the powder under different pressurization methods. The initial packing state of the powder bed will be changed by the different bed heights, which are influenced by the self-weight of the powder. Different initial packing configurations also affect the final degree of compression (Wang et al., 2022). The difference of the container aspect ratio directly leads to the different wall effect suffered by the powder bed during the compression process (Adams and McKeown, 1996; Michrafy et al., 2003). The greater the wall effect, the greater the frictional resistance, the lower the degree of compression, and the greater the B.

The function is used to describe the relationship between the variation of the normal stress and the pressurization rate in Fig. 12.

$$\sigma_z = A(1 - B^{\upsilon_p}) \tag{2}$$

Where σ_z is the normal stress (KPa), υ_p is the pressurization rate (KPa/s), A and B are parameters. The fitting parameters and correlation coefficients of the powders obtained from the fitting curves are shown in Table 4.

The physical meaning of A is the maximum equivalent normal stress at an infinite pressurization rate, depending on the particle characteristics. The larger the A, the lower the compressibility of the powder bed. The greater the equivalent stress required to achieve the same compression effect as mechanical pressurization. B is more related to compressibility, the higher the compressibility, the smaller the B. Meanwhile, B describes the sensitivity to gas–solid interaction, and the smaller the B, the more sensitive to the pressurization rate.

The relationship between compaction density and pressurization rate under gas pressurization is given by substituting equation (2) into equation (1), as shown in equation (3). This equation describes well the relationship between the compaction density and pressurization rate of the different powders under gas pressurization.

$$\frac{\rho_b}{\rho_{b,0}} = \left[\frac{A \times (1 - B^{\upsilon_p}) + \sigma_{z,0}}{\sigma_{z,0}}\right]^N \tag{3}$$

A schematic diagram of the compression process affected by different pressurization methods is given in Fig. 13. The difference compression mechanisms are illustrated with the help of this diagram and are summarized as follows:

Position of action: Under mechanical pressurization, the positive stress acts directly on the upper surface of the powder bed (local), then the force is transmitted between the particles. While under gas pressurization, the gas will directly penetrate the bed and have a compressive effect on the bed (overall).

Mode of action: In the compression process, the force of mechanical pressurization comes from the normal stress, which is continuously transferred from above and below through the contact between the particles. The powder overcomes the interparticle

Table 4
Fitting parameters and correlation coefficients.

Material	A	B	R^2
A	4.5	0.96	0.996
B	25.8	0.99	0.989
C	9.0	0.98	0.979
D	6.9	0.98	0.971
E	10.7	0.98	0.995

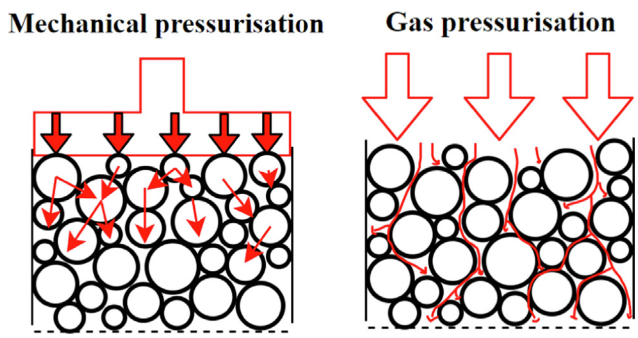

Fig. 13. Diagram of different pressurization methods affecting the compression process.

force and slips into the gap to rearrange. The gas inside is discharged, the area of contact between the particles is further increased, and the compression efficiency is improved. Unlike the former, the gas penetrates into the powder bed during the gas pressurization. The gas–solid interaction is generated and the interaction among the particles is weakened. The gas exerts a dragging force on the particles, resulting in a compression effect. Compared with mechanical pressurization, the gas penetration has an additional dominant effect on powder compression.

4. Conclusion

In summary, the effect of particle characteristics on the compression behavior of powders is studied in this paper. The compression results under mechanical and gas pressurization were compared. The results show that:

When compression reaches a steady-state, there are differences in the compressibility and RCD variations corresponding to the two pressurization methods. We propose a equation for the normal stress and the pressurization rate. The comparison of the compressibility percentages at the pressurization rate and the equivalent stress shows that the effect of gas pressurization is smaller than the mechanical pressurization. The equation was further obtained which described the relationship between the compaction density and pressurization rate of the different powders under gas pressurization.

Finally, the reasons for the different effects of mechanical pressurization and gas pressurization were analyzed from two perspectives: position and mode. Mechanical pressurization acts on the surface of the bed, and the normal stress is transmitted from top to bottom. Gas pressurization penetrates the whole bed which causes the gas to flow among the particles. Compared with mechanical pressurization, the permeability of the gas has an additional dominant effect on the powder compression, which in turn decreases the effect of gas pressurization.

CRediT authorship contribution statement

Shicheng Wang: Conceptualization, Methodology, Writing – original draft, Investigation, Writing – review & editing. **Xiaolei Guo:** Writing – review & editing, Formal analysis. **Haifeng Lu:** Visualization, Investigation, Supervision. **Haifeng Liu:** Validation, Project administration, Funding acquisition.

Data availability

The authors do not have permission to share data.

Declaration of Competing Interest

The authors declare that they have no known competing financial interests or personal relationships that could have appeared to influence the work reported in this paper.

Acknowledgments

The authors acknowledge financial supports from the National Natural Science Foundation of China (51876066) and the Shanghai Engineering Research Center of Coal Gasification (18DZ2283900).

References

Abdullah, E.C., Geldart, D., 1999. The use of bulk density measurements as flowability indicators. Powder Technology 102 (2), 151–165.
Adams, M., McKeown, R., 1996. Micromechanical analyses of the pressure-volume relationship for powders under confined uniaxial compression. Powder Technology 88 (2), 155–163.
Adolfsson, Å., Olsson, H., Nyström, C., 1997. Effect of particle size and compaction load on interparticulate bonding structure for some pharmaceutical materials studied by compaction and strength characterisation in butanol. European Journal of Pharmaceutics and Biopharmaceutics 44 (3), 243–251.
Bombac, D., Cvahte, P., Balog, M., Kugler, G., Tercelj, M., 2020. In-Depth Comparison of an Industrially Extruded Powder and Ingot Al Alloys. Metals 10 (11).
He, Y., Guo, F., 2018. Micromechanical analysis on the compaction of tetrahedral particles. Chemical Engineering Research and Design 136, 610–619.
He, Y., Li, Y.Y., Evans, T.J., Yu, A.B., Yang, R.Y., 2019. Effects of particle characteristics and consolidation pressure on the compaction of non-spherical particles. Minerals Engineering 137, 241–249.
Jenike, A.W., 1983. ANALYSIS OF SOLIDS DENSIFICATION DURING THE PRESSURIZATION OF LOCK HOPPERS, Int Symp - The Role of Part Interact in Powder Mech, August 29, 1983 - August 31, 1983. Eindhoven, Neth, pp. 131-143.
Kaerger, J.S., Edge, S., Price, R., 2004. Influence of particle size and shape on flowability and compactibility of binary mixtures of paracetamol and microcrystalline cellulose. European Journal of Pharmaceutical Sciences 22 (2–3), 173–179.
Kawakita, K., Ludde, K.H., 1971. Some considerations on powder compression equations. Powder Technology 4 (2), 61–68.
Koynov, A., Romanski, F., Cuitiño, A.M., 2013. Effects of particle size disparity on the compaction behavior of binary mixtures of pharmaceutical powders. Powder Technology 236, 5–11.
Kuhn, L.T., McMeeking, R.M., Lange, F.F., 1991. A model for powder consolidation. J. Am. Ceram. Soc. (USA) 74 (3), 682–685.
Lu, H., Guo, X., Gong, X., Cong, X., Liu, K., Qi, H., 2012a. Experimental study on aerated discharge of pulverized coal. Chemical Engineering Science 71, 438–448.
Lu, H.F., Guo, X.L., Cong, X.L., Liu, K., Sun, X.L., Xie, K., Gong, X., Lu, J., 2012b. The Discharge of Pulverized Coal from a Pressurized Aerated Hopper. Industrial & Engineering Chemistry Research 51 (42), 13839–13845.
Michrafy, A., Kadiri, M.S., Dodds, J.A., 2003. Wall friction and its effects on the density distribution in the compaction of pharmaceutical excipients. Chemical Engineering Research & Design 81 (A8), 946–952.
Richard, P., Nicodemi, M., Delannay, R., Ribiere, P., Bideau, D., 2005. Slow relaxation and compaction of granular systems. Nature Materials 4 (2), 121–128.
Saha, B.P., Kumar, V., Joshi, S.V., Balakrishnan, A., Martin, C.L., 2012. Investigation of compaction behavior of alumina nano powder. Powder Technology 224, 90–95.
Samimi, A., Hassanpour, A., Ghadiri, M., 2005. Single and bulk compressions of soft granules: Experimental study and DEM evaluation. Chemical Engineering Science 60 (14), 3993–4004.
Sharma, R., Setia, G., 2019. Mechanical dry particle coating on cohesive pharmaceutical powders for improving flowability - A review. Powder Technology 356, 458–479.
Shen, C., Li, Y., Xu, X., 2022. Analysis of the compressibility of edible powders under low pressure. Journal of Food Engineering 316.
Stasiak, M., Tomas, J., Molenda, M., Rusinek, R., Mueller, P., 2010. Uniaxial compaction behaviour and elasticity of cohesive powders. Powder Technology 203 (3), 482–488.
Sukumaran, B., Ashmawy, A.K., 2003. Influence of inherent particle characteristics on hopper flow rate. Powder Technology 138 (1), 46–50.
Tomas, J., 2004. Product design of cohesive powders - Mechanical properties, compression and flow behavior. Chemical Engineering & Technology 27 (6), 605–618.
Wang, S., Guo, X., Shen, Z., Lu, H., Liu, H., 2022. Experimental study on the alumina fine powder internal compression characteristics under gas pressurization. Powder Technology 406, 117586.
Yigit, E., 2018. A novel compressed sensing based quantity measurement method for grain silos. Computers and Electronics in Agriculture 145, 179–186.
Zeng, C.N., Wang, Y.K., 2019. Compressive behaviour of wheat from confined uniaxial compression tests. International Agrophysics 33 (3), 347–354.
Zhu, F., Zhao, J., 2021. Interplays between particle shape and particle breakage in confined continuous crushing of granular media. Powder Technology 378, 455–467.